Direct observation of the melt/substrate interface in chill-block melt spinning

Kosuke Nagashio and Kazuhiko Kuribayashi

ISAS/JAXA, Sagamihara, Kanagawa 229-8510, JAPAN

Email: nagashio@isas.jaxa.jp

The rapid solidification process in melt spinning has been empirically deduced from the relationship between the resultant phases/microstructure and the wheel speed, because the melt/substrate interface is difficult to observe directly. The controversy over whether the ribbon solidifies in or outside the melt puddle (thermal or momentum transport control) still remains unsolved. Herein, we report the first *in-situ* observation of the melt/substrate interface. The Si melt was ejected onto a silicon wafer rotated "transversely" by a vacuum motor in a chamber. The silicon wafer, which is transparent for wavelength > 1.1 μm, can be used as the chill substrate to simulate the rapid solidification on a copper substrate, since the thermal conductivity of silicon is of the same order as that of copper. Successive images captured through the silicon wafer using a high-speed infrared imaging revealed that the ribbon solidified just at the underside of the melt puddle. It was demonstrated that ribbon formation is controlled by thermal transport.

1. Introduction

Among various rapid solidification processes, the most industrially important one is melt spinning, in which a melt is ejected via a nozzle on to a rotating wheel and thereby solidifies in the form of a ribbon. It is empirically known that the cooling rate increases with decreasing ribbon thickness and therefore the material properties are dramatically improved. The first attempt to characterize the process physics was made by Kavesh [1] who proposed two limiting transport models. One is thermal transport control in which the ribbon solidifies in the melt puddle, the other is momentum transport control in which the melt film is dragged out from the melt puddle by the rotating wheel and solidifies farther downstream. Kavesh considered that thermal transport is dominant since the Prandtl number of typical metals is generally ~0.01, which indicates that thermal transport is much faster than momentum transport by viscosity. It was, however, pointed out that the solidification of ribbons is difficult in the melt puddle because of the finite thermal resistance at the melt/substrate interface [2]. Indeed, the heat transfer coefficient was assumed to be infinite in Kavesh's consideration. Therefore, there is

controversy as to whether ribbon formation is controlled by thermal [3,4] or momentum [5,6] transport.

Subsequently, many experiments were carried out to determine the heat transfer coefficient [4,7-9]. Gillen and Cantor [4] took photographs of the ribbons from the top surface and calculated the cooling rate by calibrating the photographic color density of the ribbon into temperature. Then the heat transfer coefficient was estimated to be ~10^5 Wm^{-2}K^{-1} by both Newtonian and non-Newtonian heat flow analyses. Although the ribbon thickness is 20~40 μm at most, the estimation of the heat transfer coefficient at the melt/substrate interface from the surface cooling rate still includes uncertainty. The measurements of cooling rates by the direct observation systems are summarized in Table 1. All the measurements, however, were carried out from the top or side of the melt puddle, except Tkatch et al.'s experiment using a thermocouple [10]. Recently, numerical simulation is being widely applied to melt spinning [11,12]. The heat transfer coefficient, however, is dealt with as a parameter in the calculations. Therefore, the behavior in the melt puddle is still open question although it is widely applied to the industrial materials. We report the first *in-situ* observation of the melt/substrate interface

Table 1   Summary of data for heat transfer coefficient and cooling rate obtained by the direct observation system.

researchers	Year	Alloy	Methods	dT/dt / Ks^{-1}	h / Wm^{-2}K^{-1}	Thermal/Momentum	Refs.
D.H. Warrington et al.	1981	inconel	Photograph from side	$6.3*10^4$-$1.5*10^5$	N/A	Thermal	[19]
M.J. Tenwick et al.	1985	copper	Photograph from top	$4*10^5$-$5*10^6$	0.25-$2.1*10^6$	Momentum to Thermal	[7]
A.G. Gillen et al.	1985	Ni-5wt%Al	IR photograph from top	1-$5*10^6$	$6*10^4$-$2*10^5$	Thermal	[4]
K. Takeshita et al.	1986	Ni-19at%P	IR thermometer from top	N/A	$7*10^5$-$1.3*10^6$	N/A	[8]
E. Vogt et al.	1986	Fe-6.3wt%Si	Pyrometry from top	$9.5*10^4$-$1.05*10^5$	N/A	N/A	[20]
H. Mühlbach et al.	1987	Steel	IR camera from top	$6*10^5$	$5*10^3$-10^8	N/A	[9]
G. Stephani et al.	1988	Steel	IR camera from side	$1.1*10^5$-$1.05*10^6$	N/A	(Thermal)	[21]
V. I. Tkatch et al.	1997	Fe$_{40}$Ni$_{40}$P$_{14}$B$_6$	Thermocouple from bottom	$1.8*10^5$-$3.3*10^6$	$4.5*10^4$-$4.5*10^5$	Momentum	[10]
H. Hirosawa et al.	2003	Nd$_4$Fe$_{77.5-x}$B$_{18.5}$M$_x$	IR CCD from top	1-$3.9*10^5$	N/A	N/A	[22]

in the melt puddle using a novel imaging system in order to elucidate whether ribbon formation is controlled by thermal or momentum transport.

2. Experimental Procedure

The chilled wheel rotates longitudinally in the typical configuration of the melt-spinning setup where direct observation is difficult. In the present study, an optically-polished silicon wafer with 3-inch diameter and 3-mm thickness was used as the chill substrate that was rotated transversely by a vacuum motor, as shown in Fig. 1. Silicon has a high thermal conductivity of the same order as copper and is transparent for wavelengths longer than 1.1 μm.

B-doped Si was melted in a quartz crucible by RF induction and ejected from a 1 mmϕ orifice to the rotating silicon wafer by Ar gas pressurized to 0.035 MPa. The rotation speed of the vacuum motor can be varied roughly from 500 to 50,000 rpm. The condition required for typical melt spinning was attained below 10,000 rpm. The ribbon formation process at the melt/substrate interface was directly monitored through the silicon wafer using a high-speed infrared (IR) imaging system. This system has an InSb detector with an effective wavelength range of 3~5 μm and 32×32 resolution at 5 kHz.

3. Results

Figure 2 (a) shows successive images of the melt-spinning process captured by high-speed IR imaging. The time in ms indicated above each image was set to be 0 ms for the frame immediately prior to impact. The experimental conditions were as follows. The melt superheat temperature was 73 K, the wheel speed beneath the nozzle was 25.4 m/s, the tilt angle of the silicon wafer was 15°, and the distance from the nozzle tip to the silicon wafer was 15 mm. The image at t=-4.0 ms before ejection was out of focus. After the melt was
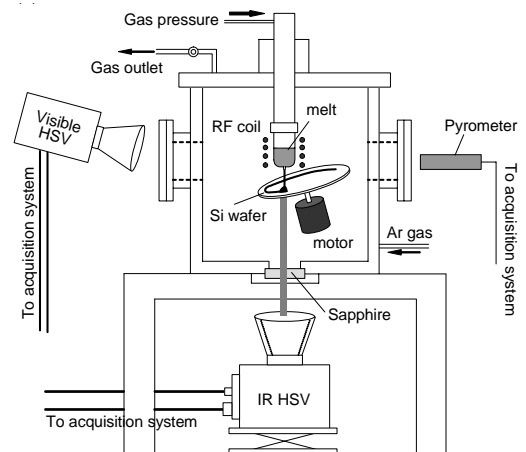

Fig.1 Schematic illustration of whole experimental apparatus for the transverse melt-spinning system.

ejected through the orifice, it approached the silicon wafer. The image at t=0, just before impact, was well focused. The solidification took place immediately after impact at t=0.2 ms. The solid was dragged toward the rotating direction (right to left) and the remaining melt spread slightly in the counter-rotating direction. After the transition period of 0<t<1.4 ms, the position of the solid/liquid interface became roughly stationary at t>1.4 ms. This indicates that the melt puddle was stably formed on the silicon wafer and the ribbon was continuously extracted from the melt puddle.

The positions of the solid/liquid and liquid/gas interfaces were traced in 20 successive images at t>1.4 ms and superimposed by white lines into a single image, as shown in Fig. 2 (b). It is evident that the ribbon formation process reached a steady state within 1.4 ms after the ejected melt impinged on the silicon wafer, since the volume of the melt supplied continuously from the nozzle balanced with that of the extracted ribbon. The center of the spreading circle of melt at steady state shifted to the right from the white dotted circle, which is the initial
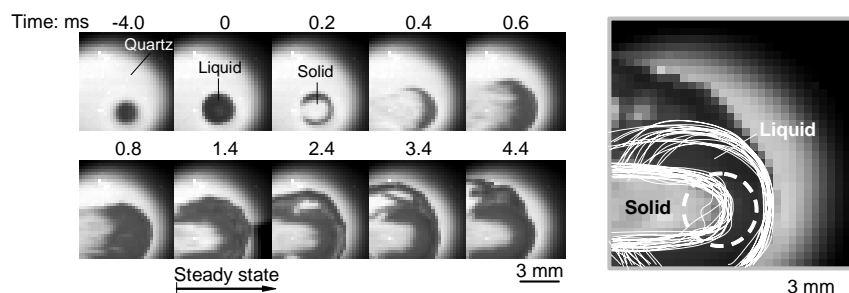

Fig. 2　(a) Successive images (32×32) at the underside of the melt puddle captured by high-speed IR imaging at 5 kHz. The time unit was ms. In these images, the solid is apparently brighter than the liquid due to the higher emissivity of the solid. At the wheel speed of 25.4 m/s, a single rotation of the silicon wafer takes 7.8 ms. (b) Representative image in which the positions of the solid/liquid and liquid/gas interfaces were traced at t>1.4 ms in (a) and superimposed. The white dotted circle is the initial position of the ejected melt just before impact (i.e. t=0 in (a)).
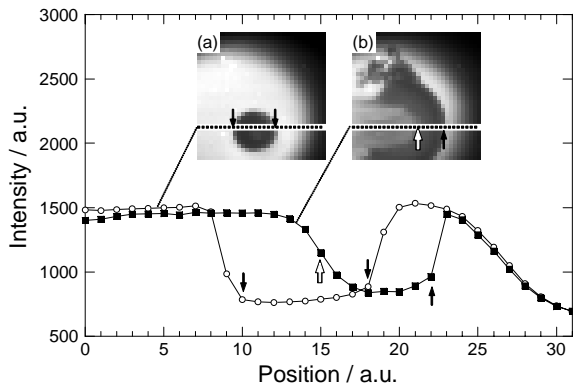
Fig. 3 Intensity profiles along dotted lines in (a) IR image just before the impact and (b) IR image at steady state. The rotation speed and tilt angle of the wafer were 25.4 m/s and 15 °, respectively.
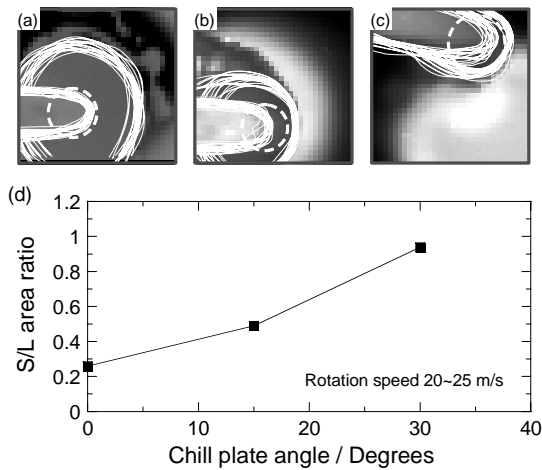

Fig. 4 IR images at steady state for different tilt angles; (a) 0 °, (b) 15 ° and (c) 30 °. Rotation speeds were roughly fixed at 20 - 25 m/s. (d) Area ratio of solid and liquid as a function of tilt angles.
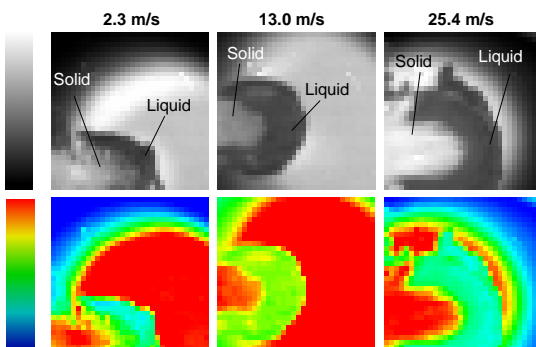

Fig. 5 Temperature uniformity within the solid region as a function of rotation speeds. The tilt angle of Si wafer was constant at 15 °. Upper images are shown in gray scale, while lower images are shown in color scale.

position of the ejected melt just before impact. This is because the melt puddle was dragged due to the rapid rotation of the chill substrate.

Figure 3 shows the intensity profiles along dotted lines in (a) IR image just before the impact and (b) IR image at steady state. Experimental conditions are the same as those in Fig. 2. The positions shown by upward and downward arrows in IR images correspond with those in the intensity profiles. The 500 difference in intensity is roughly equivalent to the 200 K difference in temperature based on the relationship between emmisivity and temperature, assuming that the solid temperature is melting point. The intensities of the melt before the impact are roughly constant at ~800, which are almost equal to those of melt within the melt puddle at steady state. That is, the spreading melt at steady state is still superheated. Moreover, the undercooling in front of the solid/liquid interface, shown by a white arrow, was not detected in the intensity profile at the steady state, even though the undercooling must exist in front of the solid/liquid interface, theoretically. This is mainly due to the low spatial resolution of the IR camera. However, the detection of the undercooling will be extremely difficult experimentally.

Next the effect of the tilt angle of the wafer on the melt puddle formation is considered. Figures 4 (a)-(c) show the IR images at steady state for different tilt angles. Rotation speeds were roughly fixed at 20 - 25 m/s. When tilt angle was increased from 0 to 30 °, the distance between the nozzle and wafer increased from 12 to 20 mm, as summarized in Table 2, due to the geometrical restriction. Therefore, it was difficult to obtain the stable melt puddle at the tilt angle of 30 ° because of the instability of the ejected melt [15]. From the images (a)-(c), the area ratio of solid and liquid was analyzed and plotted in Fig. 4 (d). When the tilt angle was zero, the melt spread considerably. With increasing the tilt angle, the spreading of the melt decreased. Finally, the ideal melt spreading condition was attained at 30 ° and the area ratio of solid and liquid became almost unity. In case of transverse rotation of the flat substrate, the tilt angle is an important factor to simulate the typical melt spinning process.

Figure 5 shows the temperature uniformity as a function of rotation speeds. The tilt angle of Si wafer was kept at 15 ° and the rotation speed was increased from 2.3 to 25.4 m/s. Even at the very low rotation speed of 2.3 m/s, solidification started just below the nozzle. In case of gray scale images, it is difficult to see the temperature uniformity within the solid region. Therefore, gray scale images were converted to color scale images in which the small intensity change results in the difference in color. It is, however, noted that the same color does not indicate the same temperature in these three images due to the different acquisition conditions. Temperature uniformity within the solid was improved considerably with increasing the
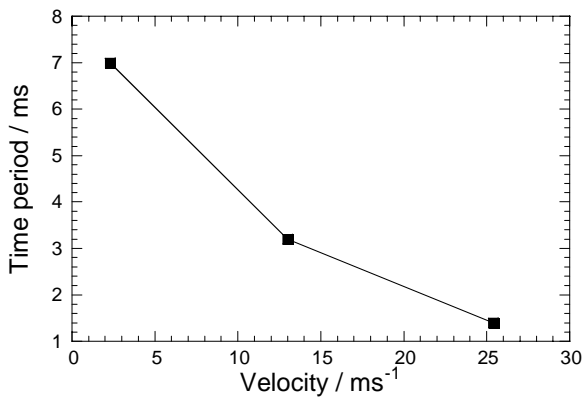
Fig. 6　Time required to reach steady state as a function of rotation speeds.

rotation speed. That is, the cooling efficiency is increased at higher rotation speed.

　　Figure 6 shows the time required to reach steady state as a function of rotation speeds. As shown in Fig. 2 (a), the solid formed first was dragged out from the melt puddle (0.4 < t < 0.8 ms) and then the solid region was formed again which resulted in steady state (t > 1.4 ms). The dragging rate depends on the rotation speed. Therefore, the time required to reach steady state decreased with increasing the rotation speeds.

4. Discussion

　　The novel IR imaging system provided the conclusive answer to the controversy whether the ribbon formation process is controlled by thermal or momentum transport. Although there was a transitive claim in which the mechanism of ribbon formation changes from momentum to thermal transport control as the rotation speed increases [7], the thermal transport was always dominant for all rotation speed regions, as shown in Fig. 5. In the present study, Si melt was used as the model material. The thermal properties of Si, especially the Prandtl number, are similar to those of typical metals. Moreover, the silicon wafer worked only as the chill plate since nucleation at the bottom surface was random in spite that Si was used for both the melt and substrate. From these facts, the present result could be extended to the typical metals, except metallic glasses in which the nucleation rate is extremely slow.

　　In the present study, the cooling rate has not been determined. The successive images in Fig. 2 (a) showed that the solidification started at the next frame of the impingement. The thickness of the solidified layer must be known in order to calculate the heat flux per unit time extracted into the chill substrate, which could not be experimentally determined from the image. Therefore,

the cooling rate could not be determined, even though the melt/substrate interface was successfully observed. Therefore, the cooling rate just at the impingement is roughly estimated as follows.

5. Conclusions

　　The novel IR imaging system was constructed in order to elucidate whether the ribbon formation process is controlled by thermal or momentum transport. We successfully monitored the melt-spinning process at the underside of the melt puddle and elucidated that thermal transport is more dominant than momentum transport for all the ranges of the rotation speed, that is, the ribbon solidifies in the melt puddle. This provides useful information for characterizing the process physics of the melt-spinning process.

References

[1]　Kavesh S. Metallic glasses, (American Society for Metals, Metals Park, Ohio, 1976), p. 36.

[2]　Shingu PH. Kobayashi K. Suzuki R. Takeshita K. in Proceedings of Rapidly quenched metals IV, (1981), pp. 57-60.

[3]　Katgerman L. Van Den Brink PJ. in Proceedings of Rapidly quenched metals IV, (1981), pp. 61-64.

[4]　Gillen AG. Cantor B. Acta metall. 1985;33:1813.

[5]　Takeshita K. Shingu PH. Trans. Japan Inst. Metals 1983;24:529.

[6]　Davies HA. in Proceedings of Rapidly quenched metals V, (1985), pp. 101-106.

[7]　Tenwick MJ. Davies HA. in Proceedings of Rapidly quenched metals V, (1985), pp. 67-70

[8]　Takeshita K. Shingu PH. Trans. JIM 1986;27:454.

[9]　Mühlbach H. Stephani G. Sellger R. Fiedler H. Int. J. Rapid Solidification 1987;3:83.

[10]　Tkatch V.I. Denisenko S.N. Beloshov O.N. Acta mater. 1997;45:2821.

[11]　Gutierrez EM. Szekely J. Metall. Trans. B 1986;17B:695.

[12]　Gong Z. Wilde P. Matthys EF. Int. J. Rapid Solidification 1991;6:1.

[19]　Warrington D.H. Davies H.A. Shohoji N. in Proceedings of Rapidly quenched metals IV, (1981), pp. 69-72.

[20]　Vogt E. Frommeyer G. in Proceedings of Rapidly solidified materials, (1986), pp. 291-296.

[21]　Stephani G. Mühlbach H. Fielder H. Richter G. Mater. Sic. Eng. 1988;98:29.

[22]　Hirosawa S. Shigemoto Y. Miyoshi T. Kanekiyo H. Scripta mater. 2003;48:839.